



# THE UNIVERSITY *of* EDINBURGH

## Edinburgh Research Explorer

### **Unsteady Ekman--Stokes dynamics: implications for surface-wave induced drift of floating marine litter**

**Citation for published version:**

Higgins, C, Vanneste, J & van den Bremer, TS 2020, 'Unsteady Ekman--Stokes dynamics: implications for surface-wave induced drift of floating marine litter', *Geophysical Research Letters*.  
<https://doi.org/10.1029/2020GL089189>

**Digital Object Identifier (DOI):**

[10.1029/2020GL089189](https://doi.org/10.1029/2020GL089189)

**Link:**

[Link to publication record in Edinburgh Research Explorer](#)

**Document Version:**

Peer reviewed version

**Published In:**

Geophysical Research Letters

**General rights**

Copyright for the publications made accessible via the Edinburgh Research Explorer is retained by the author(s) and / or other copyright owners and it is a condition of accessing these publications that users recognise and abide by the legal requirements associated with these rights.

**Take down policy**

The University of Edinburgh has made every reasonable effort to ensure that Edinburgh Research Explorer content complies with UK legislation. If you believe that the public display of this file breaches copyright please contact [openaccess@ed.ac.uk](mailto:openaccess@ed.ac.uk) providing details, and we will remove access to the work immediately and investigate your claim.



1        **Unsteady Ekman–Stokes dynamics: implications for**  
2        **surface-wave induced drift of floating marine litter**

3                **C. Higgins<sup>1,2</sup>, J. Vanneste<sup>2</sup>, T.S. van den Bremer<sup>1</sup>**

4                <sup>1</sup>Department of Engineering Science, University of Oxford, Oxford, OX1 3PJ, UK

5                <sup>2</sup>School of Mathematics and Maxwell Institute for Mathematical Sciences, University of Edinburgh,  
6                Edinburgh EH9 3FD, UK

7        **Key Points:**

- 8        • Marine litter studies include surface wave transport by Stokes drift but have ne-  
9        glected wave-induced Eulerian-mean flows in the upper ocean.  
10       • We present a model of the Eulerian-mean Ekman–Stokes response to time-varying  
11       Stokes drift for use in marine litter transport models.  
12       • Using buoy data we show that the unsteady Ekman–Stokes flow significantly al-  
13       ters both magnitude and direction of near-surface transport.

---

Corresponding author: Christopher Higgins, [christopher.higgins@keble.ox.ac.uk](mailto:christopher.higgins@keble.ox.ac.uk)

14 **Abstract**

15 We examine Stokes drift and wave-induced transport of floating marine litter on the sur-  
 16 face of a rotating ocean with a turbulent mixed layer. Due to Coriolis–Stokes forcing and  
 17 surface wave stress, a second-order Eulerian-mean flow forms, which must be added to  
 18 the Stokes drift to obtain the correct wave-induced Lagrangian velocity. We show that  
 19 this wave-driven Eulerian-mean flow can be expressed as a convolution between the un-  
 20 steady Stokes drift and an ‘Ekman–Stokes kernel’. Using this convolution we calculate  
 21 the unsteady wave-driven contribution to particle transport. We report significant dif-  
 22 ferences in both direction and magnitude of transport when the Eulerian-mean Ekman–  
 23 Stokes velocity is included.

24 **Plain Language Summary**

25 In transport models for floating marine litter, surface wave effects are often included by  
 26 simply superimposing their Stokes drift (the small net drift induced by waves) upon wind-  
 27 driven flows and currents. However, due to Earth’s rotation and turbulent dissipation  
 28 in the ocean’s surface mixed layer, the Stokes drift also drives additional Eulerian-mean  
 29 flows. To obtain the correct transport velocity, the wave-induced Eulerian-mean flow must  
 30 be added to the Stokes drift. We develop a model that enables estimation of this wave-  
 31 induced Eulerian-mean flow from measurements or predictions of the wave field and ap-  
 32 ply our model to buoy data. Accounting for the wave-induced Eulerian-mean flow sig-  
 33 nificantly alters predictions of transport of floating marine litter by waves.

34 **1 Introduction**

35 Floating marine debris, including plastic pollution, has rapidly become one of the  
 36 most pressing environmental problems (Eriksen et al., 2014), particularly for marine ecosys-  
 37 tems (Lavender Law, 2017). Although consensus exists about the longevity of plastic in  
 38 the marine environment (Andrady, 2011) and the relatively large buoyancy of a signif-  
 39 icant share of plastic produced (Geyer et al., 2017), with both factors contributing to  
 40 their long-distance transport, the total plastic budget of the world’s oceans is poorly un-  
 41 derstood. A significant mismatch exists between the estimated amount of land-generated  
 42 plastic that enters coastal waters (5–12 million tonnes yr<sup>−1</sup>, Jambeck et al. (2015)) and  
 43 the estimated total amount of plastic floating at sea (less than 0.3 million tonnes, Cózar  
 44 et al. (2014); Eriksen et al. (2014); van Sebille et al. (2015)). Similarly, the amount of  
 45 plastics measured at sea over the last few decades (Lebreton et al., 2019; Ostle et al., 2019;  
 46 Wilcox et al., 2020) has not kept pace with growth in global plastic production (Gold-  
 47 stein et al., 2012; Geyer et al., 2017). To understand this mismatch, an improved under-  
 48 standing of the physical processes governing transport and dispersion is required (van  
 49 Sebille et al., 2020). This letter focuses on one of these processes: surface waves.

50 As a particle undergoes its periodic motion beneath surface waves, it experiences  
 51 a Lagrangian-mean velocity in the waves’ direction known as Stokes drift (Stokes, 1847).  
 52 More generally, Stokes drift is the difference between the average Lagrangian velocity  
 53 of a fluid parcel and the average Eulerian velocity of the fluid measured at a fixed spa-  
 54 tial location (e.g. Bühler (2014); van den Bremer & Breivik (2017)). Surface gravity waves  
 55 on the open ocean are mostly caused by winds. At any location and time, the wave field  
 56 is a superposition of waves that have been generated by earlier winds at another loca-  
 57 tion. Wave models, such as WAM (The WAMDI Group, 1988) and WaveWatch-III (Tol-  
 58 man, 2009), have been developed to predict wave fields and thus Stokes drift (Webb &  
 59 Fox-Kemper, 2011; Breivik et al., 2014).

60 A recent and growing body of literature is examining the role of Stokes drift in the  
 61 transport and dispersion of floating plastic pollution. Iwasaki et al. (2017) showed that  
 62 in the Sea of Japan, Stokes drift pushed microplastics closer to the coast. Delandmeter

63 & van Sebille (2019) and Onink et al. (2019) report a similar result in Arctic regions.  
 64 Dobler et al. (2019) demonstrated that Stokes drift fundamentally changes transport pat-  
 65 terns in the South Indian Ocean by shifting the convergence regions to the west, caus-  
 66 ing leakage into the South Atlantic rather than the South Pacific. Waves may also al-  
 67 low particles to cross strong circumpolar winds and currents (Fraser et al., 2018).

68 Crucially, the above studies have simply superimposed the Stokes drift obtained  
 69 from the local wave field onto the Eulerian current field obtained from ocean general cir-  
 70 culation models or observations. In doing so, they have ignored the fact that the Eule-  
 71 rian flow is itself modified by surface waves: on the rotating Earth, the Coriolis force as-  
 72 sociated with the Stokes drift drives an Eulerian-mean current in the turbulent upper-  
 73 ocean boundary layer (Ursell, 1950; Hasselmann, 1970; Xu & Bowen, 1994; Lewis & Belcher,  
 74 2004), as noted in Onink et al. (2019). Together with the Stokes drift and the non-wave  
 75 background flow, this wave-induced Eulerian current forms the Lagrangian velocity with  
 76 which marine litter is transported. It is this wave-induced Eulerian current, which we  
 77 call the Ekman–Stokes flow, that this letter examines.

78 We derive a model for computing the unsteady Eulerian-mean Ekman–Stokes re-  
 79 sponse to a time-varying Stokes drift, taking into account the correct wave stress bound-  
 80 ary condition and the Coriolis–Stokes forcing. We do so for the case of constant eddy  
 81 viscosity in the turbulent upper-ocean layer and a quasi-monochromatic (or narrow-banded)  
 82 wave field, and zero initial wave-induced Eulerian-mean velocity  $\bar{\mathbf{u}} = \mathbf{0}$ . The product  
 83 of this letter is an Ekman–Stokes convolution kernel, which can readily be used to pre-  
 84 dict the wave-induced Eulerian-mean flow in the turbulent upper-ocean boundary layer  
 85 and hence the Lagrangian transport of floating marine debris. This kernel is a low-computa-  
 86 tion-cost alternative to fully-coupled general circulation and wave models, which include  
 87 the effect of waves in both the Coriolis–Stokes forcing and the surface boundary condi-  
 88 tion (Breivik et al., 2015). Using sample wave field data from buoys, we show that ac-  
 89 counting for the Eulerian-mean Ekman–Stokes response to a time-varying Stokes drift  
 90 considerably alters the trajectories of drifting objects.

## 91 2 Unsteady Ekman–Stokes flow

We consider a homogeneous (constant-density), incompressible ocean of constant  
 depth  $d$ , described by horizontal coordinates  $x$  and  $y$ , and a vertical coordinate  $z$  mea-  
 sured upwards from the undisturbed water level. The governing equations, divided through  
 by the (constant) density  $\rho$ , are

$$\partial_t \mathbf{u} + \mathbf{u} \cdot \nabla \mathbf{u} + \mathbf{f} \times \mathbf{u} = -\nabla p + \nu \nabla^2 \mathbf{u}, \quad \nabla \cdot \mathbf{u} = 0, \quad (1a)$$

$$w|_{z=\eta} = \partial_t \eta + \mathbf{u}_H|_{z=\eta} \cdot \nabla_H \eta, \quad \hat{\mathbf{n}} \cdot \vec{\boldsymbol{\tau}} \cdot \hat{\mathbf{s}}|_{z=\eta} = 0, \quad (1b)$$

$$w|_{z=-d} = 0, \quad (1c)$$

92 where  $z = \eta(x, y, t)$  denotes the free surface elevation,  $\mathbf{u}$  is the three-dimensional ve-  
 93 locity vector,  $\mathbf{f}$  the Coriolis vector,  $\mathbf{A}_H \equiv (A_x, A_y, 0)$  the horizontal component of any  
 94  $\mathbf{A}$ , and  $\vec{\boldsymbol{\tau}}$  the stress tensor with components  $\tau_{ij} = -(p - p_0)\delta_{ij} + \nu(\partial_i u_j + \partial_j u_i)$ , with  
 95  $p_0$  the atmospheric pressure divided by the (constant) density  $\rho$  and  $\nu$  the turbulent eddy  
 96 viscosity, taken constant. The unit vectors  $\hat{\mathbf{n}}$  and  $\hat{\mathbf{s}}$  are normal and tangential to the free  
 97 surface respectively, so (1b) is a stress-free condition.

### 98 2.1 Wave-averaged mean-flow equations

99 We assume the wave steepness is small,  $\alpha \equiv kA \ll 1$ , where  $A$  is the peak wave  
 100 amplitude of  $\eta$  and  $k$  the peak wavenumber, and solve (1) to  $O(\alpha^2)$  using a Stokes ex-  
 101 pansion  $\mathbf{u} = \mathbf{u}_1 + \mathbf{u}_2 + \dots$ , where the subscript denotes the order in  $\alpha$ . We focus on  
 102 deep-water waves ( $kd \gg 1$ ).

103 Linear wave dynamics arises at  $O(\alpha)$ , where we ignore viscous effects, neglecting  
 104 a thin vorticity boundary layer of thickness  $\delta_\nu = \sqrt{2\nu/\omega}$  under the (generally satisfied)  
 105 assumption  $k\delta_\nu \ll 1$ . Consequently, we ignore viscous damping of waves as they prop-  
 106 agate. In contrast, the Coriolis force must be retained since, as demonstrated by Has-  
 107 selmann (1970),  $O(f/\omega)$  corrections put horizontal and vertical velocity components out  
 108 of quadrature, with impact on the wave-averaged dynamics.

Integrating the  $O(\alpha^2)$  equations over a wave period, we obtain the wave-averaged  
 mean flow equations (e.g. Huang, 1979; Suzuki & Fox-Kemper, 2016)

$$\partial_t \bar{u} - f v_L = -\partial_x \bar{p} + \nu \nabla^2 \bar{u}, \quad \partial_t \bar{v} + f u_L = -\partial_y \bar{p} + \nu \nabla^2 \bar{v}, \quad (2a)$$

$$\partial_t \bar{w} = -\partial_z \bar{p} + \nu \nabla^2 \bar{w}, \quad \partial_x \bar{u} + \partial_y \bar{v} = -\partial_z \bar{w}, \quad (2b)$$

109 where the overbar denotes a time average,  $\mathbf{u}_L = \bar{\mathbf{u}} + \mathbf{u}_S$  is the Lagrangian (or particle-  
 110 transport) velocity associated with the waves, with  $\bar{\mathbf{u}} = \bar{\mathbf{u}}_2$  the wave-induced Eulerian-  
 111 mean velocity and  $\mathbf{u}_S$  the Stokes drift, and the horizontal component of the Coriolis vec-  
 112 tor introduces only higher-order corrections to the flow. To derive (2a) and (2b) we as-  
 113 sumed that the non-wave background flow has small Rossby number,  $|\nabla \times \mathbf{u}_B|/f \ll$   
 114 1. It follows that the corresponding Stokes vortex force  $(\nabla \times \mathbf{u}_B) \times \mathbf{u}_S$  is negligible com-  
 115 pared with the Coriolis–Stokes term, while  $(\nabla \times \bar{\mathbf{u}}) \times \mathbf{u}_S$  is  $O(\alpha^4)$  since it involves only  
 116 the wave-induced flow (Suzuki & Fox-Kemper, 2016). The background  $\mathbf{u}_B$  can then sim-  
 117 ply be superimposed on the wave-induced Lagrangian flow  $\mathbf{u}_L$ . Where the condition  $|\nabla \times$   
 118  $\mathbf{u}_B|/f \ll 1$  does not hold – for example, in a submesoscale front – a more complete treat-  
 119 ment of the governing equations is required (e.g. McWilliams & Fox-Kemper, 2013).

120 Without the shear and pressure terms, equations (2a) and (2b) correspond to those  
 121 considered by Hasselmann (1970). The equations include the Coriolis–Stokes forcing  $-f\hat{\mathbf{z}} \times$   
 122  $\mathbf{u}_S$  (Hasselmann, 1970; Polton et al., 2005) which drives an Eulerian ‘anti-Stokes flow’,  
 123 cancelling the Stokes drift and exciting inertial oscillations, and explains Ursell (1950)’s  
 124 prediction of zero net drift for periodic waves in a rotating frame.

We focus on the horizontal momentum equations (2a) in the Stokes layer, that is,  
 the top  $O(k^{-1})$ -deep layer of the ocean where the Stokes drift and hence the Coriolis–  
 Stokes forcing are localised. One of the boundary conditions is provided by averaging  
 the condition of zero tangential stress in (1b) (Longuet-Higgins (1953), Ünlüata & Mei  
 (1970), Xu & Bowen (1994) and Seshasayanan & Gallet (2019)); it is given by

$$\partial_z \bar{\mathbf{u}}_H|_{z=0} = \partial_z \mathbf{u}_{SH}|_{z=0}. \quad (3)$$

125 Examining the viscous but non-rotating case, Longuet-Higgins (1953) showed that vor-  
 126 ticity is transported from the viscous boundary layers into the fluid interior, affecting  
 127 the mass transport profile (Ünlüata & Mei, 1970; Xu & Bowen, 1994; Seshasayanan &  
 128 Gallet, 2019). Within these boundary layers the flow is not irrotational, resulting in a  
 129 viscous stress upon the Eulerian-mean flow. Upon expanding the second equation in (2b)  
 130 about  $z = 0$ , performing a momentum budget, and averaging over a wave period, this  
 131 leads to condition (3). Additional Eulerian-mean wave-induced transport, known as boundary-  
 132 layer streaming, occurs in the boundary layer (e.g. Grue & Kolaas (2017)). The contri-  
 133 butions of Hasselmann (1970) and Longuet-Higgins (1953) (and the theory of wind-driven  
 134 currents of Ekman (1905)) were unified by Xu & Bowen (1994) into a model of wave (and  
 135 wind-) driven flow in finite-depth water.

In the Stokes layer, vertical gradients dominate over horizontal ones. It follows from  
 (2b) that the vertical velocity component and pressure gradient can be neglected. In-  
 troducing the complex notation  $\mathcal{U} = \bar{u} + i\bar{v}$  as in Huang (1979), we obtain the Ekman–  
 Stokes equations

$$(\partial_t + if - \nu \partial_z^2) \mathcal{U} = -if \mathcal{U}_S(\mathbf{x}, z, t), \quad \partial_z \mathcal{U} = \partial_z \mathcal{U}_S(\mathbf{x}, z, t) \Big|_{z=0}, \quad \lim_{z \rightarrow -\infty} \mathcal{U} = 0, \quad (4a,b,c)$$

136 where the boundary conditions follow from (3) and the requirement that the solution be  
 137 matched to a weak Eulerian flow outside the Stokes layer. The Eulerian Ekman–Stokes  
 138 velocity solving (4) is driven by the Stokes drift in two ways, via the Coriolis–Stokes forc-  
 139 ing in the fluid interior (Polton et al., 2005) and via the wave stress (4b).

140 Note that a wind stress could be added to (4b); by linearity, the wind-driven Ek-  
 141 man velocity would be superimposed in convolution form on the wave-driven velocity  
 142 we obtain (e.g. Madsen (1978) Eq. (21) for linearly-varying  $\nu(z)$ ). In a coupled oceanic-  
 143 atmospheric model, Lewis & Belcher (2004) derive steady solutions to (4) for non-constant  
 144 viscosity, though they do not seem to include the wave stress.

## 145 2.2 Solution by Laplace transform

We solve (4) by Laplace transform, assuming that the Stokes drift  $\mathcal{U}_s$  has a time-  
 independent vertical structure  $\exp(2kz)$  corresponding to a quasi-monochromatic wave  
 field, but an otherwise arbitrary time dependence. Denoting the Laplace transform by  
 a tilde, with

$$\tilde{g}(s) = \mathcal{L}\{g(t)\} = \int_0^\infty g(t)e^{-st}dt, \quad g(t) = \mathcal{L}^{-1}\{\tilde{g}(s)\} = \frac{1}{2\pi i} \int_{\gamma-i\infty}^{\gamma+i\infty} \tilde{g}(s)e^{st}ds, \quad (5a,b)$$

where  $\gamma$  is a real number such that the contour path of integration is in the region of con-  
 vergence of  $\tilde{g}(s)$ , we find that when  $\mathcal{U}(t=0) = 0$

$$\tilde{\mathcal{U}} = 2k \left( 1 + \frac{if}{s + if - 4k^2\nu} \right) \frac{\tilde{\mathcal{U}}_s e^{z\sqrt{(s+if)/\nu}}}{\sqrt{(s+if)/\nu}} - \frac{if\tilde{\mathcal{U}}_s e^{2kz}}{s + if - 4k^2\nu}. \quad (6)$$

146 This is the sum of a particular solution – the second term – which can be interpreted  
 147 as a partial anti-Stokes flow varying over the Stokes depth  $\delta_s = (2k)^{-1}$ , and a homo-  
 148 geneous solution – the first term – varying over the Ekman depth  $\delta_E = \sqrt{2\nu/f}$ , which  
 149 includes a contribution driven by the vertical shear of the anti-Stokes flow through bound-  
 150 ary condition (4b) (second term in the brackets in (6)).

A special case of (6) occurs if  $\mathcal{U}_s$  approaches a steady value  $\overline{\mathcal{U}}_s$  as  $t \rightarrow \infty$ . Then  
 $\tilde{\mathcal{U}}$  tends to the time-independent solution (cf. Seshasayanan & Gallet (2019))

$$\overline{\mathcal{U}} = \frac{(1-i)D}{2} \overline{\mathcal{U}}_s \left( 1 + \frac{1}{1+iD^2/2} \right) e^{(1+i)z/\delta_E} - \frac{\overline{\mathcal{U}}_s e^{2kz}}{1+iD^2/2}, \quad (7)$$

151 where  $D \equiv \delta_E/\delta_s$  is the fixed ratio of Ekman to Stokes depths. In the limit  $D \rightarrow 0^+$ ,  
 152 equation (7) approaches  $-\overline{\mathcal{U}}_s \exp(2kz)$ : up to an inertial oscillation this is the so-called  
 153 ‘anti-Stokes’ Eulerian-mean flow, predicted by Hasselmann (1970) to be induced by pe-  
 154 riodic waves in a rotating, inviscid ocean. Viscosity acts to reduce the shear in the anti-  
 155 Stokes flow, so that a nonzero Lagrangian-mean velocity remains.

## 156 2.3 Ekman–Stokes kernel

We now use the Laplace convolution theorem to write the unsteady solution for the  
 Ekman–Stokes mean flow as a function of time for arbitrary Stokes drift as

$$\mathcal{U}(\mathbf{x}, z, t) = \mathcal{U}_s|_{z=0} * K(z, t), \quad (8)$$

where  $*$  denotes convolution in time and

$$K(z, t) = \mathcal{L}^{-1} \left\{ \frac{2ke^{z\sqrt{(s+if)/\nu}}}{\sqrt{(s+if)/\nu}} + \frac{if}{s + if - 4k^2\nu} \left( \frac{2ke^{z\sqrt{(s+if)/\nu}}}{\sqrt{(s+if)/\nu}} - e^{2kz} \right) \right\}. \quad (9)$$

The convolution kernel  $K(z, t)$ , which we will term the Ekman–Stokes kernel, can be eval-  
 uated by deforming the integration contour involved in the inverse Laplace transform

Limit	Behaviour	Theory
$t \rightarrow \infty$	$2k\sqrt{\nu}e^{-ift}/\sqrt{\pi t} [1 - if/(4k^2\nu) (1 - (1 + 2k^2z^2)/(4k^2\nu t))]$	long-time limit
$t \rightarrow 0^+$	$8\nu k^2\delta(z/\delta_s) - ife^{2kz}$	short-time limit
$\nu \rightarrow 0^+$	$-ife^{-ift}e^{2kz}$	Hasselmann (1970)
$f \rightarrow 0^+$	$2k\sqrt{\nu}e^{-z^2/(4\nu t)}/\sqrt{\pi t}$	Longuet-Higgins (1953)

**Table 1.** Asymptotic behaviour of the Ekman–Stokes kernel  $K(z, t)$ .

to obtain (see supplementary material)

$$K(z, t) = 2k\sqrt{\nu}e^{-ift}\frac{e^{-z^2/(4\nu t)}}{\sqrt{\pi t}} - ife^{(4k^2\nu - if)t}\sum_{\pm}\frac{e^{\pm 2kz}}{2}\operatorname{erfc}\left(\sqrt{4k^2\nu t} \pm \frac{z}{\sqrt{4\nu t}}\right), \quad (10)$$

where  $\sum_{\pm}$  denotes the sum of the plus and minus terms and the complementary error function  $\operatorname{erfc}(x) = 1 - \operatorname{erf}(x)$ . An equivalent form emphasising dependence on wave parameters uses the scaled error function  $\operatorname{erfcx}(t) = e^{t^2}\operatorname{erfc}(t)$  and reads

$$K(z, t) = 2k\sqrt{\nu}e^{-ift}\frac{e^{-z^2/(4\nu t)}}{\sqrt{\pi t}} - ife^{-ift}\frac{e^{-z^2/(4\nu t)}}{2}\sum_{\pm}\operatorname{erfcx}\left(\sqrt{4k^2\nu t} \pm \frac{z}{\sqrt{4\nu t}}\right). \quad (11)$$

157 The Ekman–Stokes kernel  $K$  captures the (Eulerian-mean) flow response to the Stokes  
 158 drift. The  $1/\sqrt{t}$  describes the establishment of an Ekman spiral driven by the wave stress;  
 159 the  $if$  terms describe the impact of the Coriolis–Stokes forcing. Note that the dimen-  
 160 sion of  $K(z, t)$  is time<sup>-1</sup>.

Several limits of the kernel are of interest; they are given in dimensional terms in Table 1. The limits  $\nu \rightarrow 0^+$  and  $f \rightarrow 0^+$  are best understood by rewriting (11) in terms of the dimensionless parameters  $D = \delta_e/\delta_s$ ,  $\zeta = 2kz$  and  $\tau = ft$  to obtain

$$K(\zeta, \tau)/f = De^{-i\tau}\frac{e^{-\zeta^2/(2D^2\tau)}}{\sqrt{2\pi\tau}} - \frac{i}{2}\sum_{\pm}e^{-i\tau - \zeta^2/(2D^2\tau)}\operatorname{erfcx}\left(D\sqrt{\frac{\tau}{2}} \pm \frac{\zeta}{\sqrt{2D^2\tau}}\right). \quad (12)$$

161 When  $D \gg 1$ , e.g. because  $f \rightarrow 0^+$ , the Coriolis–Stokes sum term in (12) is negli-  
 162 gible and the flow becomes the Longuet-Higgins (1953) response to the wave stress at the  
 163 surface. In contrast, for  $D \ll 1$ , e.g. as  $\nu \rightarrow 0^+$ , the anti-Stokes result of Hasselmann  
 164 (1970) is approached non-uniformly in  $\zeta$ . This singular behaviour arises since for any  $D \neq$   
 165 0 the shear condition at the surface cannot be met by an exact anti-Stokes flow, so in  
 166 a thin layer of depth  $\sim \sqrt{\nu/f}$  near the surface cancellation of the Stokes drift is imper-  
 167 fect (e.g. Seshasayanan & Gallet (2019)). Over long times  $\tau \rightarrow \infty$ , the Coriolis–Stokes  
 168 terms decay on the viscous rather than the inertial timescale, despite being caused by  
 169 Earth’s rotation.

170 The magnitude and argument of the dimensionless kernel  $K(\zeta, \tau)$  are shown in Fig-  
 171 ure 1 for  $D = 1$ . The magnitude is largest towards  $(\tau, \zeta) = (0, 0)$  due to the singular  
 172 behaviour discussed above. The kernel has the character of an amplitude-decaying in-  
 173 ertial oscillation with period  $2\pi/f$  with an orientation in the horizontal plane that os-  
 174 cillates with the inertial period. Equation (11) together with the convolution in time (8)  
 175 is the key result of this letter. Taking as inputs a time series of Stokes drift and estimates  
 176 of the peak wavenumber  $k$ , Coriolis parameter  $f$  and turbulent viscosity  $\nu$ , these equa-  
 177 tions produce a time series of the associated (Eulerian-mean) Ekman–Stokes current at  
 178 any vertical elevation  $z$ , which can simply be added to the Stokes drift time series to give  
 179 the Lagrangian-mean current relevant for marine litter transport. An open-source im-  
 180 plementation in Python is provided as supplementary material.



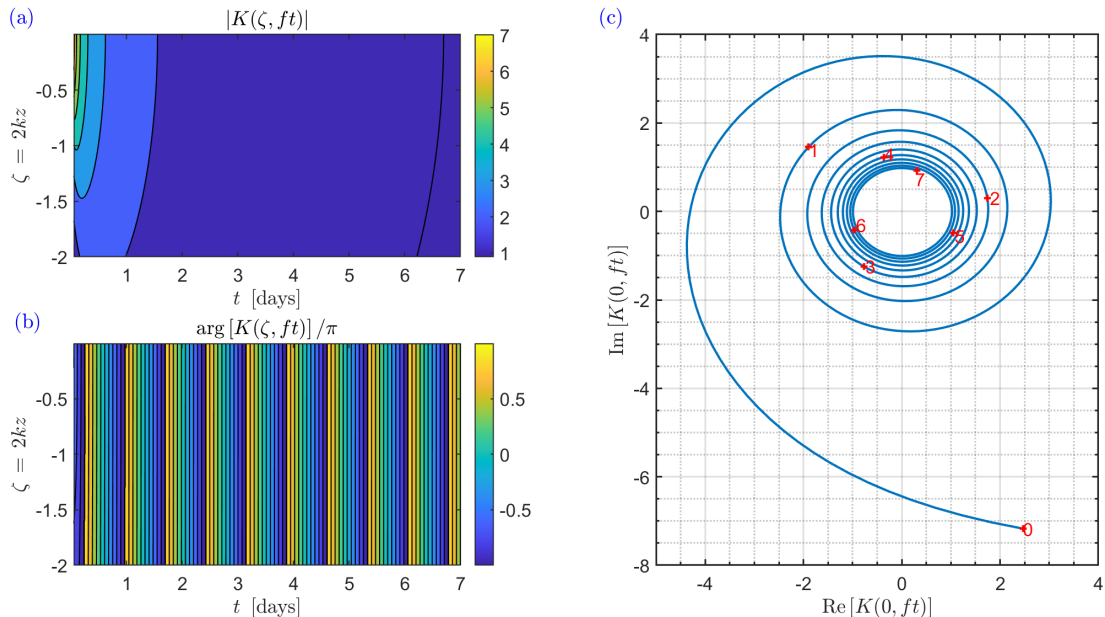


**Figure 1.** Ekman–Stokes kernel  $K(\zeta, \tau)$  for  $D = 1$  (with  $f = 1 \times 10^{-4} \text{s}^{-1}$ ): (a) magnitude and (b) argument as a function of depth and time, and (c) hodograph at the surface ( $\zeta = 0$ ) with time (in days) shown in red. In panel (a) we have saturated the colour scale, as the kernel is singular at  $(\zeta, \tau) = (0, 0)$ .

### 3 Sample calculations of the Ekman–Stokes flow

#### 3.1 Idealised storm

To demonstrate the use of the Ekman–Stokes kernel, we calculate the Eulerian response to an idealised Gaussian storm lasting approximately 24 hours. Specifically, we set  $u_s(z = 0) = u_s^* \exp(-(t - t^*)^2/(\sigma^2))$  (and  $v_s = 0$ ) with  $\sigma = 6$  hrs and magnitude  $u_s^* = 0.070$  m/s being reached at  $t^* = 24$  hrs. Choosing  $f = 1.0 \times 10^{-4} \text{s}^{-1}$  and  $\nu = 1.0 \times 10^{-2} \text{m}^2 \text{s}^{-1}$  ( $D = 1.1$ ), we set  $\mathcal{U}(z = 0, t = 0) = 0$  and evaluate the response for 1 week.

In figure 2 we plot the  $u$  and  $v$  components and magnitudes, respectively, of the second-order currents over a week-long period. The sum of Stokes drift (black) and Ekman–Stokes flow (blue) gives the Lagrangian velocity (red). Beneath, wave roses are plotted for these second-order currents. The angular direction corresponds to the angle of propagation of the flow (separated into 30 bins), the radius of each bar represents the percentage of time during which the velocity has a given direction, and the colour scale divides the data into velocity amplitude ranges. Fig. 2 shows that the Stokes drift is reduced by a (delayed) partial ‘anti-Stokes’ flow, a transverse component arises on the same time scale, and damped inertial oscillations are formed which remain after the storm has ceased. The resulting Lagrangian current is deflected by the large transverse component of the Ekman–Stokes flow, to the right in the Northern Hemisphere (and to the left in the Southern Hemisphere).



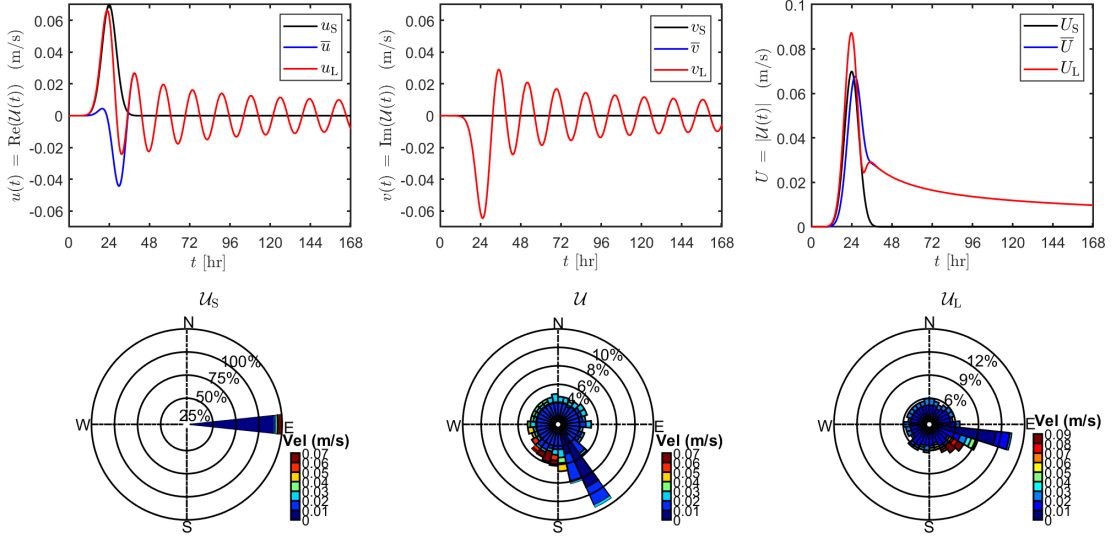


**Figure 2.** **Top:** Time series of wave-induced velocities formed in response to an idealised 24-hr Gaussian storm in the Northern Hemisphere showing the two components and magnitude of the Stokes drift  $U_s$  (black), Eulerian-mean velocity  $U$  (blue) and Lagrangian velocity  $U_L$  (red). **Bottom:** Wave roses for  $U_s$ ,  $U$ , and  $U_L$ , with radial distance representing the fraction of time during which the velocity has a given direction, and colour indicating magnitude in m/s.

201

### 3.2 Buoy data

We use half-hourly records for the San Nicolas Island buoy ( $33.22^\circ$  N,  $119.88^\circ$  W) obtained from CDIP (the Coastal Data Information Project) and estimate the Stokes drift using the formula

$$U_s = g^{-1} \omega_p^3 A_p^2 \exp(2\bar{k}z) \exp(i\theta_p), \text{ where } A_p = H_s / (2\sqrt{2}). \quad (13)$$

202

203

204

205

206

207

208

where  $\theta_p$  is the peak wave direction,  $H_s$  the significant wave height, and  $\omega_p$  the peak frequency calculated from the peak period  $T_p$ . By making a quasi-monochromatic approximation, we assume the wavenumber spectrum is peaked about  $k = \text{mean}(k_p) = \text{mean}(\omega_p^2/g)$ , to leading order. We integrate (11) using the Stokes drift (13) by a trapezoidal rule with time-step equal to the buoy sampling time. Defining the surface value of the kernel as  $\lim_{z \rightarrow 0^-} K(z, t)$  instead of directly setting  $z = 0$  allows the singular behaviour at  $(0, 0)$  to be avoided.

209

210

211

212

213

214

215

216

As in figure 2, the top panels of figure 3 show  $u$  and  $v$  components and magnitudes of the second-order currents. The largest Stokes drift at San Nicolas Island over this time period is in a South-Southeasterly direction, though a share of very small values arising from small-amplitude waves are also seen to propagate West-Southwest (cf. bottom-left panel, figure 3). In contrast, the Ekman–Stokes contribution is much more directionally-spread at all velocity amplitudes due to excited inertial oscillations. Superimposing the two flows leads to a directionally-spread Lagrangian drift which veers to the right of the Stokes drift.

217

218

To find the displacement associated with the unsteady flows, we take the wavenumber and Stokes drift time series to be uniform in space, which is valid for the relatively

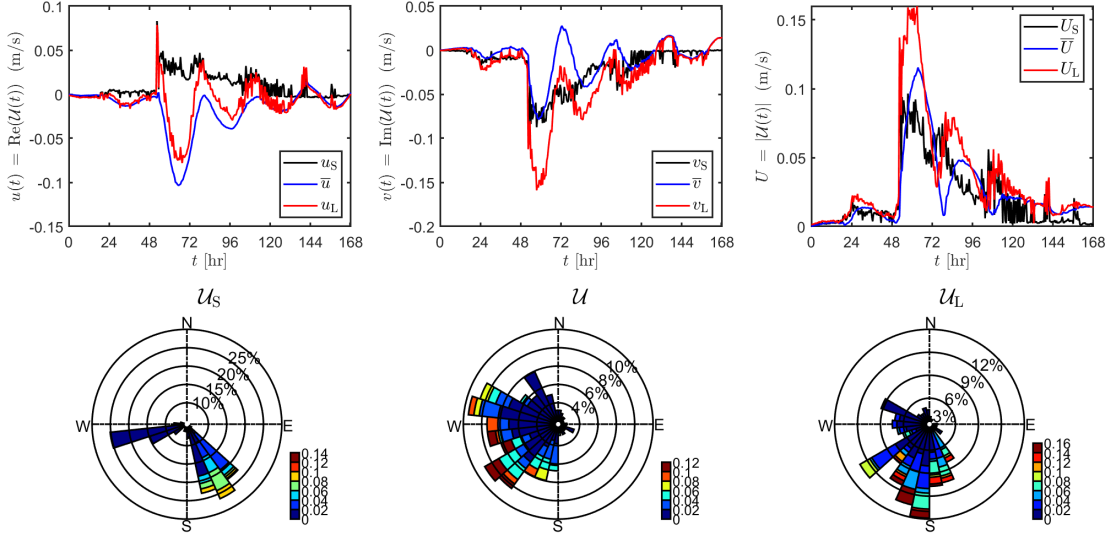


**Figure 3.** **Top:** Time series (14/05/00 15:41 – 22/05/00 09:41 UTC) of wave-induced velocities computed from buoy data from San Nicolas Island ( $33.22^\circ$  N,  $119.88^\circ$  W), with colours as in Fig. 2. **Bottom:** Corresponding wave roses, as in Fig. 2.

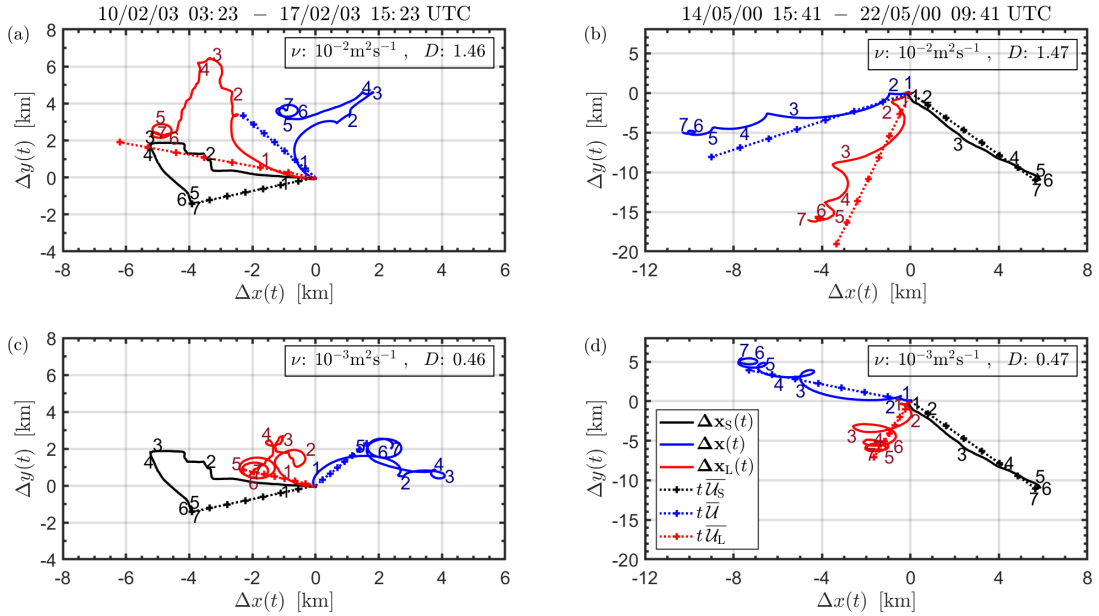


**Figure 4.** Particle paths at the surface ( $z=0$ ) computed for the San Nicolas Island buoy using our Ekman–Stokes convolution kernel. **Columns:** two different time samples. **Rows:** different values of turbulent viscosity. Paths shown are obtained using the Stokes drift (black), Eulerian-mean velocity (blue) and Lagrangian-mean velocity (red). Dashed lines ignore time-dependence of the Stokes drift and show the steady response to the average of the Stokes drift over the periods considered. All paths begin at  $(\Delta x, \Delta y) = (0, 0)$ . Numbers beside each line denote the number of days elapsed.

219 small accumulated displacements considered. Particle displacements computed by time-  
 220 integrating the velocities obtained from our Ekman–Stokes kernel are plotted in figure  
 221 4. Panels (a) and (c) show displacements over one week in February 2003 and (b) and  
 222 (d) over a week in May 2000, with (b) corresponding to velocities plotted in figure 3. Line  
 223 colours are consistent with figures 2 and 3. Straight dotted lines represent steady solu-  
 224 tions, i.e. (7) multiplied by time elapsed, with  $\overline{U}_s = \text{mean}(U_s)$ . Evidently, the steady  
 225 approximation causes errors in the prediction of net particle displacement. Instead of  
 226 following the black trajectory described by the Stokes drift alone, we predict the par-  
 227 ticle will follow the red trajectory, being transported by the Lagrangian velocity, the sum  
 228 of the Stokes drift and wave-induced Ekman–Stokes flow. For both time samples, the  
 229 Lagrangian displacement is to the right of the Stokes displacement, as for the velocities  
 230 (in the Southern Hemisphere, it will lie to the left).

231 We anticipate that the realistic range for eddy viscosity is  $O(10^{-3})$ – $O(10^{-2})$   $\text{m}^2\text{s}^{-1}$ ,  
 232 estimated from the vertical mixing coefficient  $S_M = 0.30$  in Mellor & Blumberg (2004)  
 233 by using the law of the wall. Comparing (c) and (d) with (a) and (b), particle displace-  
 234 ment is reduced and inertial oscillations more pronounced for the smaller viscosity  $\nu =$   
 235  $10^{-3}\text{m}^2\text{s}^{-1}$  in (c) and (d), since the anti-Stokes flow increases in magnitude as viscos-  
 236 ity decreases. For the realistic range of  $\nu$  the displacement is significantly altered in both  
 237 magnitude and direction when the Ekman–Stokes flow is included.

## 238 4 Discussion and conclusions

239 Our analysis has demonstrated the need to add a so-called Ekman–Stokes flow to  
 240 the Stokes drift to properly estimate the wave-induced Lagrangian-mean flow which trans-  
 241 ports floating marine litter. We have derived an Ekman–Stokes convolution kernel which  
 242 can readily be used to predict the wave-induced Eulerian-mean flow in the turbulent upper-  
 243 ocean boundary layer. It integrates three important effects: the surface wave stress, the  
 244 Coriolis–Stokes forcing, and unsteadiness of the forcing and response.

245 We properly account for the viscous wave stress at the surface. This is often ne-  
 246 glected (e.g. Lewis & Belcher (2004); Polton et al. (2005); Onink et al. (2019)), though  
 247 it may be of similar magnitude to the wind stress. Including the wave stress should yield  
 248 more accurate predictions of the Lagrangian drift, particularly when wind and waves are  
 249 misaligned. Our model also incorporates the Coriolis–Stokes forcing which induces a par-  
 250 tial anti-Stokes flow and alters the response over the Ekman depth  $\delta_E = \sqrt{2\nu/f}$  (cf.  
 251 Polton et al. (2005)). Our results demonstrate that for realistic eddy viscosities  $10^{-3}$ –  
 252  $10^{-2}$   $\text{m}^2\text{s}^{-1}$  the Stokes drift is only partially cancelled by an anti-Stokes flow. Perhaps  
 253 most importantly, our approach shows that unsteadiness of the Stokes drift and induced  
 254 Eulerian response can be readily incorporated into models of Lagrangian drift using a  
 255 simple convolution. As passage times of storms are typically  $O(1/f)$ , accounting for time  
 256 variability is crucial for accurate predictions of drift.

257 Future work should improve our model in the following four ways. First, for sim-  
 258 plicity we have assumed a constant eddy viscosity, although our kernel approach could  
 259 be adapted for linearly-increasing eddy viscosity (Madsen (1977), Lewis & Belcher (2004)),  
 260 which provides a more accurate representation of turbulence in the upper-ocean bound-  
 261 ary layer. Second, Shrira & Almelah (2020) have presented a solution method incorpo-  
 262 rating time-dependence of the eddy viscosity due to processes such as mixed-layer re-  
 263 stratification or wave breaking (Price & Sundermeyer, 1999). Parameterisations of tur-  
 264 bulent viscosity should thus account for both time and depth variation.

265 Third, while we have used a quasi-monochromatic assumption in our model, the  
 266 Ekman–Stokes kernel can in principle be applied to broad-banded spectra using an ad-  
 267 ditional integration over frequency. For typical broad-banded spectra, the near-surface  
 268 Stokes drift is more strongly sheared than for a monochromatic wave corresponding to

269 the peak frequency (Webb & Fox-Kemper, 2011). Therefore, the wave stress dominates  
 270 the forcing of the Eulerian-mean flow whose magnitude is strengthened and whose di-  
 271 rection becomes more aligned with that of the Stokes drift, as we have confirmed in pre-  
 272 liminary computations. We emphasise that the wave stress is proportional to the fifth  
 273 moment of the frequency spectrum and hence ill-defined for most empirical spectra, whose  
 274 high-frequency tails behave like  $\omega^{-4}$  or  $\omega^{-5}$  (Breivik et al., 2016). This indicates a high  
 275 sensitivity of the wave-induced mean flow to the spectral tail, suggesting the need for  
 276 a careful assessment of the form of this tail and of its impact on the Eulerian-mean dy-  
 277 namics. We note that Seshasayanan & Gallet (2019) recently showed that the steady Ekman-  
 278 Stokes current is unstable to perturbations. Future work should consider the importance  
 279 of this instability in the real ocean and how it might interact with unsteadiness of the  
 280 wave-induced flow.

281 Fourth, ocean transport can be modelled using the tracer equation rather than La-  
 282 grangian tracking methods (Dobler et al., 2019; Wu et al., 2019). Stokes advection plays  
 283 an important role in strong wind/wave conditions, and affects up/down-welling in coastal  
 284 regions (Suzuki & Fox-Kemper, 2016; Wu et al., 2019). We anticipate that including the  
 285 unsteady Ekman-Stokes flow will cause variations in up/down-welling velocities over timescales  
 286  $\gtrsim O(1/f)$  (§4(i) Hasselmann, 1970; McWilliams & Restrepo, 1999)

## 287 Acknowledgments

288 T.S. v.d.B. was supported by a Royal Academy of Engineering Research Fellow-  
 289 ship, J.V. by the UK Natural Environment Research Council grant NE/R006652/1. The  
 290 authors thank Harry Cunningham for assistance writing the Python script in the sup-  
 291 plementary material. The authors are grateful to Ø. Breivik for advice on how to ob-  
 292 tain representative values of viscosity.

293 Buoy data was obtained from the Coastal Data Information Program (CDIP) ([https://  
 294 cdip.ucsd.edu](https://cdip.ucsd.edu)). Data corresponding to the time series used in this paper is available  
 295 in the supplementary material.

296 The authors thank two referees whose comments have improved this paper and en-  
 297 riched the discussion of future work in §4.

## 298 References

- 299 Andradý, A. L. (2011). Microplastics in the marine environment. *Mar. Pollut. Bull.*,  
 300 *62*(8), 1596-1605. doi: 10.1016/j.marpolbul.2011.05.030
- 301 Breivik, O., Bidlot, J., & Janssen, P. (2016). A stokes drift approximation based on  
 302 the phillips spectrum. *Ocean Modelling*, *100*, 49-56. doi: [https://doi.org/10.1016/  
 303 j.ocemod.2016.01.005](https://doi.org/10.1016/j.ocemod.2016.01.005)
- 304 Breivik, O., Janssen, P., & Bidlot, J.-R. (2014). Approximate Stokes drift profiles in  
 305 deep water. *J. Phys. Oceanogr.*, *44*(9), 2433-2445. doi: 10.1175/JPO-D-14-0020.1
- 306 Breivik, O., Mogensen, K., Bidlot, J.-R., Balmaseda, M. A., & Janssen, P. (2015).  
 307 Surface wave effects in the NEMO ocean model: Forced and coupled experiments.  
 308 *J. Geophys. Res.: Oceans*, *120*(4), 2973-2992. doi: 10.1002/2014JC010565
- 309 Bühler, O. (2014). *Waves and mean flows* (2nd ed.). Cambridge University Press,  
 310 Cambridge, UK.
- 311 Cózar, A., Echevarría, F., González-Gordillo, J. I., Irigoien, X., Úbeda, M.,  
 312 Hernández-León, S., ... Duarte, C. M. (2014). Plastic debris in the open ocean.  
 313 *Science*, *111*(28), 10239-10244. doi: 10.1073/pnas.1314705111
- 314 Delandmeter, P., & van Sebille, E. (2019). The parcels v2.0 Lagrangian framework:  
 315 new field interpolation schemes. *Geosci. Model Dev.*, *12*(8), 3571-3584. doi: 10  
 316 .5194/gmd-12-3571-2019

- 317 Dobler, D., Huck, T., Maes, C., Grima, N., Blanke, B., Martinez, E., & Arduin,  
318 F. (2019). Large impact of Stokes drift on the fate of surface floating de-  
319 bris in the South Indian Basin. *Marine Pollution Bulletin*, *148*, 202-209. doi:  
320 doi.org/10.1016/j.marpolbul.2019.07.057
- 321 Ekman, V. W. (1905). On the influence of the Earth's rotation on ocean-currents.  
322 *Ark. Mat. Astron. Fys.*, *2*(11), 1-53.
- 323 Eriksen, M., Lebreton, L. C. M., Carson, H. S., Thiel, M., Moore, C. J., Borro,  
324 J. C., ... Reisser, J. (2014). Plastic pollution in the world's oceans: More than 5  
325 trillion plastic pieces weighing over 250,000 tons afloat at sea. *PLoS ONE*, *9*(12),  
326 e111913. doi: 10.1371/journal.pone.0111913
- 327 Fraser, C., Morrison, A., Hogg, A. M., Macaya, E., van Sebille, E., Ryan, P.,  
328 ... Waters, J. (2018). Antarctica's ecological isolation will be broken by  
329 storm-driven dispersal and warming. *Nature Climate Change*, *8*(8). doi:  
330 10.1038/s41558-018-0209-7
- 331 Geyer, R., Jambeck, J. R., & Lavender Law, K. (2017). Production, use, and fate of  
332 all plastics ever made. *Sci. Adv.*, *3*(7), e1700782. doi: 10.1126/sciadv.1700782
- 333 Goldstein, M. C., Rosenberg, M., & Cheng, L. (2012). Increased oceanic microplas-  
334 tic debris enhances oviposition in an endemic pelagic insect. *Biol. Lett.*, *8*, 817-20.  
335 doi: 10.1098/rsbl.2012.0298
- 336 Grue, J., & Kolaas, J. (2017). Experimental particle paths and drift velocity in steep  
337 waves at finite water depth. *J. Fluid Mech.*, *810*, R1. doi: 10.1017/jfm.2016.726
- 338 Hasselmann, K. (1970). Wave-driven inertial oscillations. *Geophys. Fluid Dyn.*, *1*,  
339 463-502. doi: 10.1080/03091927009365783
- 340 Huang, N. E. (1979). On surface drift currents in the ocean. *J. Fluid Mech.*, *91*(1),  
341 191-208. doi: 10.1017/S0022112079000112
- 342 Iwasaki, S., Isobe, A., Kako, S., Uchida, K., & Tokai, T. (2017). Fate of microplas-  
343 tics and mesoplastics carried by surface currents and wind waves: A numerical  
344 model approach in the Sea of Japan. *Marine Pollution Bulletin*, *121*(1), 85-96.  
345 doi: doi.org/10.1016/j.marpolbul.2017.05.057
- 346 Jambeck, J. R., Geyer, R., Wilcox, C., Siegler, T. R., Perryman, M., Andrady, A.,  
347 ... Lavender Law, K. (2015). Plastic waste inputs from land into the ocean.  
348 *Science*, *347*(6223), 768-771. doi: 10.1126/science.1260352
- 349 Lavender Law, K. (2017). Plastics in the marine environment. *Annu. Rev. Mar. Sci.*,  
350 *9*, 205-229. doi: 10.1146/annurev-marine-010816-060409
- 351 Lebreton, L., Egger, M., & Slat, B. (2019). A global mass budget for positively  
352 buoyant macroplastic debris in the ocean. *Sci. Rep.*, *9*, 12922. doi: 10.1038/s41598-  
353 -019-49413-5
- 354 Lewis, D., & Belcher, S. (2004). Time-dependent, coupled, Ekman boundary layer  
355 solutions incorporating Stokes drift. *Dynam. Atmosph. and Oceans*, *37*(4), 313-  
356 351. doi: doi.org/10.1016/j.dynatmoce.2003.11.001
- 357 Longuet-Higgins, M. S. (1953). Mass transport in water waves. *Phil. Trans. Roy.*  
358 *Soc. London A*, *245*(903), 535-581. doi: 10.1098/rsta.1953.0006
- 359 Madsen, O. S. (1977). A realistic model of the wind-induced ekman boundary  
360 layer. *J. Phys. Oceanogr.*, *7*(2), 248-255. doi: 10.1175/1520-0485(1977)007<0248:  
361 ARMOTW>2.0.CO;2
- 362 Madsen, O. S. (1978). Mass transport in deep-water waves. *J. Phys. Oceanogr.*,  
363 *8*(6), 1009-1015. doi: 10.1175/1520-0485(1978)008<1009:MTIDWW>2.0.CO;2
- 364 McWilliams, J. C., & Fox-Kemper, B. (2013). Oceanic wave-balanced surface fronts  
365 and filaments. *J. Fluid Mech.*, *730*, 464-490. doi: 10.1017/jfm.2013.348
- 366 McWilliams, J. C., & Restrepo, J. M. (1999). The wave-driven ocean circu-  
367 lation. *J. Phys. Oceanogr.*, *29*(10), 2523-2540. Retrieved from [https://](https://doi.org/10.1175/1520-0485(1999)029<2523:TWD0C>2.0.CO;2)  
368 [doi.org/10.1175/1520-0485\(1999\)029<2523:TWD0C>2.0.CO;2](https://doi.org/10.1175/1520-0485(1999)029<2523:TWD0C>2.0.CO;2) doi:  
369 10.1175/1520-0485(1999)029(2523:TWD0C)2.0.CO;2
- 370 Mellor, G., & Blumberg, A. (2004). Wave breaking and ocean surface layer thermal

- 371 response. *J. Phys. Oceanogr.*, *34*(3), 693-698. doi: 10.1175/2517.1
- 372 Onink, V., Wichmann, D., Delandmeter, P., & van Sebille, E. (2019). The  
373 role of Ekman currents, geostrophy, and Stokes drift in the accumulation of  
374 floating microplastic. *J. Geophys. Res.: Oceans*, *124*(3), 1474-1490. doi:  
375 10.1029/2018JC014547
- 376 Ostle, C., Thompson, R., Broughton, D., Gregory, L., Wootton, M., & Johns, D. G.  
377 (2019). The rise in ocean plastics evidenced from a 60-year time series. *Nat.*  
378 *Commun.*, *10*, 1622. doi: 10.1038/s41467-019-09506-1
- 379 Polton, J., Lewis, D., & Belcher, S. (2005). The role of wave-induced Coriolis-Stokes  
380 forcing on the wind-driven mixed layer. *J. Phys. Oceanogr.*, *35*(4), 444-457. doi:  
381 10.1175/JPO2701.1
- 382 Price, J. F., & Sundermeyer, M. A. (1999). Stratified Ekman layers. *J. Geophys.*  
383 *Res.: Oceans*, *104*(C9), 20467-20494. doi: 10.1029/1999JC900164
- 384 Seshasayanan, K., & Gallet, B. (2019). Surface gravity waves propagating in a rotat-  
385 ing frame: The Ekman-Stokes instability. *Phys. Rev. Fluids*.
- 386 Shrira, V. I., & Almelah, R. B. (2020). Upper-ocean Ekman current dynamics: a  
387 new perspective. *J. Fluid Mech.*, *887*, A24. doi: 10.1017/jfm.2019.1059
- 388 Stokes, G. G. (1847). On the theory of oscillatory waves. *Trans. Cam. Phil. Soc.*, *8*,  
389 441-455.
- 390 Suzuki, N., & Fox-Kemper, B. (2016). Understanding Stokes forces in the wave-  
391 averaged equations. *J. Geophys. Res.: Oceans*, *121*(5), 3579-3596. doi: 10.1002/  
392 2015JC011566
- 393 The WAMDI Group. (1988). The wam model-a third generation ocean wave predic-  
394 tion model. *J. Phys. Oceanogr.*, *18*(12), 1775-1810. doi: 10.1175/1520-0485(1988)  
395 018(1775:TWMTGO)2.0.CO;2
- 396 Tolman, H. L. (2009). User manual and system documentation of WAVEWATCH III  
397 TM version 3.14 Technical Note.
- 398 Ünlüata, U., & Mei, C. C. (1970). Mass transport in water waves. *J. Geophys. Res.*,  
399 *75*(36), 7611-7618. doi: 10.1029/JC075i036p07611
- 400 Ursell, F. (1950). On the theoretical form of ocean swell on a rotating earth.  
401 *Mon. Not. Roy. Astron. Soc., Geophys. Suppl.*, *6*(s1), 1-8. doi: 10.1111/  
402 j.1365-246X.1950.tb02968.x
- 403 van den Bremer, T. S., & Breivik, O. (2017). Stokes drift. *Phil. Trans. Roy. Soc.*  
404 *London A*, *376*(2111). doi: 10.1098/rsta.2017.0104
- 405 van Sebille, E., Aliani, S., Law, K. L., Maximenko, N., Alsina, J., A. Bagaev,  
406 M. B., . . . Wichmann, D. (2020). The physical oceanography of the trans-  
407 port of floating marine debris. *Environ. Res. Lett.*, *15*(2), 023003. doi:  
408 10.1088/1748-9326/ab6d7d
- 409 van Sebille, E., Wilcox, C., Lebreton, L., Maximenko, N., Hardesty, B. D., van  
410 Franeker, J. A., . . . Lavender Law, K. (2015). A global inventory of small floating  
411 plastic debris. *Environ. Res. Lett.*, *10*(12), 124006. doi: 10.1088/1748-9326/10/12/  
412 124006
- 413 Webb, A., & Fox-Kemper, B. (2011). Wave spectral moments and Stokes drift esti-  
414 mation. *Ocean Modelling*, *40*(3), 273-288. doi: doi.org/10.1016/j.ocemod.2011.08  
415 .007
- 416 Wilcox, C., Hardesty, B. D., & K., L. L. (2020). Abundance of floating plastic par-  
417 ticles is increasing in the western North Atlantic Ocean. *Envir. Sci. Tech.*, *54*(2),  
418 790-796. doi: 10.1021/acs.est.9b04812
- 419 Wu, L., Staneva, J., Breivik, O., Rutgersson, A., George Nurser, A., Clementi, E.,  
420 & Madec, G. (2019). Wave effects on coastal upwelling and water level. *Ocean*  
421 *Modelling*, *140*, 101405. doi: https://doi.org/10.1016/j.ocemod.2019.101405
- 422 Xu, Z., & Bowen, A. (1994). Wave- and wind-driven flow in water of finite depth.  
423 *J. Phys. Oceanogr.*, *24*(9), 1850-1866. doi: 10.1175/1520-0485(1994)024(1850:  
424 WAWDFI)2.0.CO;2